Diamond & Related Materials 123 (2022) 108857

Contents lists available at ScienceDirect

Diamond & Related Materials

journal homepage: www.elsevier.com/locate/diamond

Radial growth kinetics of epitaxial pyrolytic carbon layers deposited on carbon nanotube surfaces by non-catalytic pyrolysis

Fan Liu *, Naoto Nishioka, Fumio Ogawa, Toshiyuki Hashida

Fracture and Reliability Research Institute, Tohoku University, 6-6-11, Aza-Aoba, Aramaki, Aobaku, Sendai, Miyagi 980-8579, Japan

ARTICLE INFO

Keywords:
Carbon nanotube
Chemical vapor deposition
Vapor growth

ABSTRACT

Chemical vapor deposition of pyrolytic carbon (PyC) onto carbon nanotube (CNT) surfaces by hydrocarbon pyrolysis can thicken the nanotube diameter until the desirable size. Vapor-induced thickening of CNTs may require no metal catalysts because the CNT-templated growth can easily convert PyC deposits into epitaxial graphene shells. However, little work has been done on the kinetics of the vapor-induced CNT thickening process during the non-catalytic pyrolysis. In this study, we discuss the growth mechanism of epitaxial PyC layers on CNT surfaces achieved by the low-pressure (≤1.5 kPa) pyrolysis of ethylene, which is distinct from previous studies using much higher gas pressures (4–100 kPa) for the PyC deposition. The average thickness of deposited PyC layers is calculated by analyzing the transmission electron microscopy images of PyC-coated CNTs. The crystallinity of PyC-coated CNTs is evaluated by Raman spectroscopy and X-ray diffraction. The thickness of PyC layers on CNT surfaces can be adjusted by simply changing the growth time under typical pyrolysis parameters (800 °C-1.5 kPa of ethylene). We find a two-stage nonlinear behavior to describe the growth kinetics of PyC layers, indicating that the radial growth rate of PyC layers can be influenced by the number of surface active sites. This study reveals the self-assembly mechanism of graphitic layers on the CNT template, which is expected to promote the diameter-controlled synthesis of CNTs.

1. Introduction

Multi-walled carbon nanotubes (MWCNTs) possess varying mechanical, thermal, and electrical properties when CNT diameters change [1,2], which is important for tailoring the CNT properties. Tremendous efforts [3–5] have been devoted to the diameter-control of CNTs by changing catalyst sizes and processing parameters during the chemical vapor deposition (CVD) synthesis. However, the production of different-sized catalyst nanoparticles may need a complicated procedure such as particle suspension, spray and dry, oxidation treatment due to the different CVD catalyst systems [6]. An alternative way for the diameter-control of CNTs is to deposit pyrolytic carbon (PyC) layers onto CNT outer surfaces by non-catalytic pyrolysis of hydrocarbon. The CNT-templated growth can easily convert the PyC deposits into epitaxial graphene shells, which offers an opportunity to adjust the wall number (diameter) of nanotubes. Nevertheless, little work has been done on the kinetics of the vapor-induced CNT thickening process during the non-catalytic pyrolysis of hydrocarbon.

The following studies have reported the phenomenon of the vapor-induced CNT thickening under various pyrolysis conditions. Feng et al. [7] used in-situ simultaneous thermal analysis technique to analyze the PyC deposits on CNT surfaces under acetylene pyrolysis at 600–700 °C, 4–9 kPa. 82% of the reaction products are proved to be graphene, and the remaining 18% are amorphous carbon. Zheng et al. [8] proposed a layer-by-layer growth model of PyC-coated CNTs under 800–1000 °C, 20 kPa of propane, mentioning that polyaromatic hydrocarbon molecules (PAHs) from the gas phase are adsorbed onto CNT surfaces via π-π stacking interactions. However, the radial growth rate of PyC layers has not been quantitatively discussed in their work. Recently, Krasnikov et al. [9] reported the formation of lateral carbon deposits on CNT surfaces after the pyrolysis (650–750 °C, 10–70 kPa of ethylene). The corresponding chemical reaction was reported to be the collision of surface-adsorbed carbon species such as C_2H_5· and C_2H_3· radicals. Monthioux et al. [10] reported the deposition of PyC layers on CNT surfaces under the pyrolysis of methane, in which hydrocarbon droplets were formed in the gas phase at high temperatures (1100–1295 °C) and high pressures (~100 kPa). All the aforementioned studies pyrolyzed the carbon sources at high pressures (4–100 kPa) to produce PyC-coated

* Corresponding author.
E-mail address: fan.liu@rift.mech.tohoku.ac.jp (F. Liu).

https://doi.org/10.1016/j.diamond.2022.108857
Received 11 November 2021; Received in revised form 26 December 2021; Accepted 18 January 2022
Available online 26 January 2022

CNTs, in which the deposited PyC layers usually exhibit a disordered microstructure. In comparison, our recent work [11] has achieved the epitaxial growth of PyC layers on defective CNT surfaces via the ethylene pyrolysis at 700–900 °C using a much lower pressure (0.5 kPa). We found that the PyC layers epitaxially grown at low pressures exhibit a well-aligned microstructure of graphitizable carbons. The crystallinity of PyC layers seems sensitive to the deposition thickness, but its reason is not yet understood. Thus, it is important to investigate the self-assembly mechanism and growth kinetics of PyC layers deposited on CNT surfaces during the low-pressure pyrolysis of ethylene.

In this paper, the relations between the microstructures of PyC-coated CNTs and the pyrolysis parameters have been systematically investigated. Diverse morphologies of PyC-coated CNTs were observed by transmission electron microscopy (TEM). The crystallinity of PyC-coated CNTs was investigated by Raman spectroscopy and X-ray diffraction (XRD). The relationship between the deposition thickness of PyC layers and growth time indicates a nonlinear two-stage behavior, including a growth rate-decaying stage and a growth rate-increasing stage. Accordingly, we propose a new model to interpret the two-stage radial growth kinetics and the corresponding microstructures of PyC-coated CNTs, in which the blocking or regeneration of available active sites on the carbon substrate is important.

2. Experimental procedure

2.1. As-received CNTs

CVD-grown carbon nanotube sheets (LINTEC OF AMERICA, INC., Nano-Science & Technology Center) were used as a pristine CNT sample in this study. The outer diameter of CNTs is about 10 nm, and the size of the CNT sheets is approximately 50 mm × 20 mm × 10 μm with 50 stacking layers.

2.2. Deposition of pyrolytic carbon onto as-received CNTs by non-catalytic pyrolysis

Before the vapor deposition of pyrolytic carbon on CNTs, the as-received CNT sheets have been purified by the hydrogen-annealing treatment in a tube furnace at 900 °C for 1 h, using a previously reported method [12] to minimize the amount of surface-adsorbed amorphous carbon. After the purification, the CNT sheets were placed in a quartz tube reactor for the pyrolysis treatment, using ethylene (C_2H_4) as the carbon source. The furnace was heated to the predetermined temperature in 20 min in vacuum, and then C_2H_4 and argon were introduced. The pressure level in our study was controlled by the flow rate ratio of C_2H_4 to argon (keeping the total flow rate at 500 sccm and the total chamber pressure at 2.5 kPa). After specific durations of time, the reactor was purged by the flowing argon at 800 sccm, and then cooled down to the room temperature. Because of the highly porous nature of CNT sheets drawn from arrays, the spacing of intertube voids was reported to be hundreds of nanometers [13]. The relatively large intertube distance in porous CNT sheets is conducive for gas diffusion so that the PyC deposition may not be limited by the mass-transport [14,15]. The penetration of hydrocarbon molecules inside the CNT sheets during the pyrolysis is considered to be sufficient for the carbon supply.

2.3. Materials characterization

XRD was performed using an X-ray diffractometer (Rigaku, SmartLab) with a Cu Kα target ($\lambda = 0.154$ nm), and the continuous scan (0.5°/min) was conducted in the range between 15° and 50°. Raman spectra were obtained by a spectrometer (Chromex, Inc250) with the laser excitation wavelength of 532 nm. Raman measurements (50× magnification) were carried out under ambient conditions, and we measured 6 points at different locations across each CNT sample. TEM samples were prepared by dispersing a small amount of CNTs in ethanol solution; sonication lasted for 5–10 min. A droplet of dispersed nanotubes was deposited on a copper grid, then CNT morphology was observed using TEM (JEOL, JEM-2100) under 200 kV at an exposure time of less than 1.5 s. At least 50 measurements were taken from TEM pictures using the image processing software (ImageJ) to calculate the average diameter of each sample. Most previous studies [8,15,16] estimated the deposition thickness of PyC layers only from the difference of CNT outer diameters, without considering a possible difference of CNT inner diameters. In order to calculate the thickness of PyC layers, here we suggest simultaneously analyzing the outer and inner diameters of PyC-coated CNTs in comparison with those of pristine CNTs. Details of the diameter measurement are shown in Fig.S1 (Supplementary material). The radial growth rate of PyC layers (nm/min) is calculated on the basis of deposition thickness and growth time.

3. Results and discussion

The empirical relation between the morphologies of PyC-coated CNTs and the pyrolysis parameters (pyrolysis temperature, ethylene pressure, growth time) is shown in Fig. 1. The TEM image of pristine CNTs (Fig. 1a) shows the irregular lattice fringe, indicating the existence of structural defects (e.g., vacancies). Figs.1b–f indicate the influence of pyrolysis temperature on the morphologies of PyC-coated CNTs when the temperature increases from 700 °C to 850 °C (fixing the ethylene pressure at 1.5 kPa and growth time at 2 h). Note that in Fig. 1 the outline of pristine CNTs based on the average outer diameter has been roughly marked by the white dashed line so that we can distinguish the newly deposited PyC layers more easily. The deposition thickness of PyC layers increases significantly with the temperature. But some disordered microstructures can be seen in the PyC-coated sample grown at 825 °C (Fig. 1e), probably due to the intensive vapor deposition at relatively high temperatures [8].

The influence of ethylene pressure on the morphologies of PyC-coated CNTs is shown by Figs.1g∼k when the ethylene pressure increases from 0.05 kPa to 1 kPa (fixing the pyrolysis temperature at 900 °C and growth time at 0.5 h). The PyC layers grown at 0.05 kPa show the graphene nanosheets that have not been curled into CNT walls (Fig. 1g). Such a phenomenon has been reported in [17], mentioning that under the ultra-low pressure of gas precursors the seamless nanotube structure may not be obtained. In contrast, Figs.1h∼k exhibit the morphologies of vapor-thickened CNTs with a rough surface, which can be attributed to the formation of nanoislands (lateral pyrolytic carbon deposits) [18].

We made a statistical analysis of the outer diameters (D) and inner diameters (d) using the TEM images of different CNT samples. The diameter distribution histograms of the pristine CNT and all the PyC-coated CNTs are shown in Fig.S2 (Supplementary material). The outer and inner diameter of PyC-coated CNTs are plotted as a function of pyrolysis temperature and ethylene pressure, respectively (Figs.2a∼b). As Fig. 2a shows, the outer diameter of PyC-coated CNTs increases rapidly with the temperature, which is consistent with the previous reports [19,20]. From Fig. 2b, the outer diameter of PyC-coated CNTs is nearly proportional to the ethylene pressure, probably due to the effect of carbon concentration on the growth rate [21]. Also, the average inner diameter of nearly all the PyC-coated CNTs has slightly decreased compared to that of pristine CNTs, but the dependence of temperature or pressure on the CNT inner diameter is not clear yet. We notice the localized bending of graphitic layers in some PyC-coated CNT samples (Fig.S3, Supplementary material). We infer that the residual stress may be accumulated during the deposition process, due to the different thermal expansion coefficients between the deposited PyC layers and the pristine CNT substrate [22,23]. Presumably the shrinkage effect [24] of deposited PyC layers might induce the bending of pristine CNT substrate, which can explain the decrease of average inner diameter. By

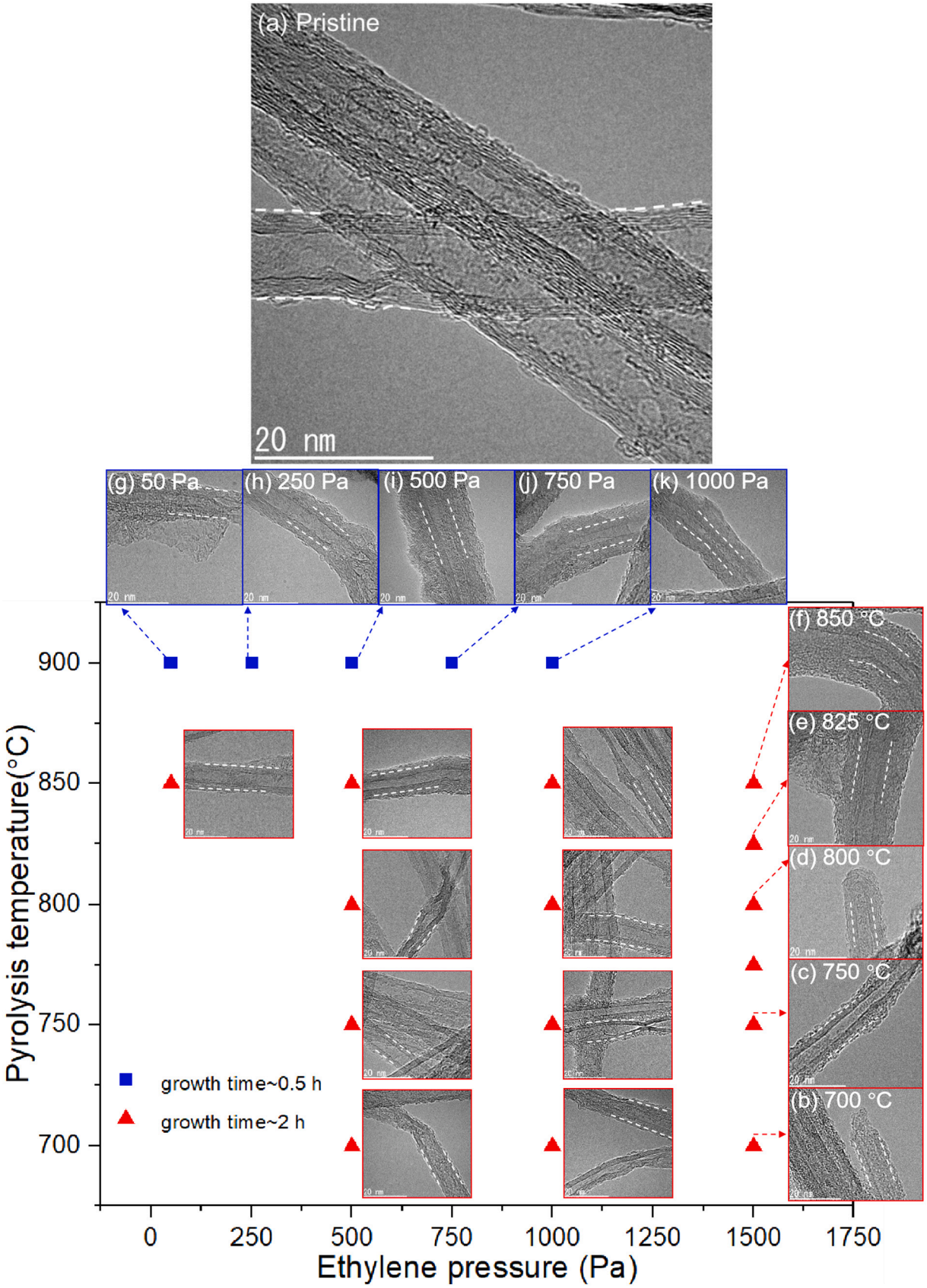

Fig. 1. (a) The TEM image of pristine CNTs as a reference; (b) ~ (k) TEM images of the PyC-coated CNTs obtain from different pyrolysis parameters: 700–900 °C, 0.05–1.5 kPa of ethylene, the growth time is 0.5 h (blue square) or 2 h (red triangle). The white dashes roughly mark the outline of the pristine CNT.

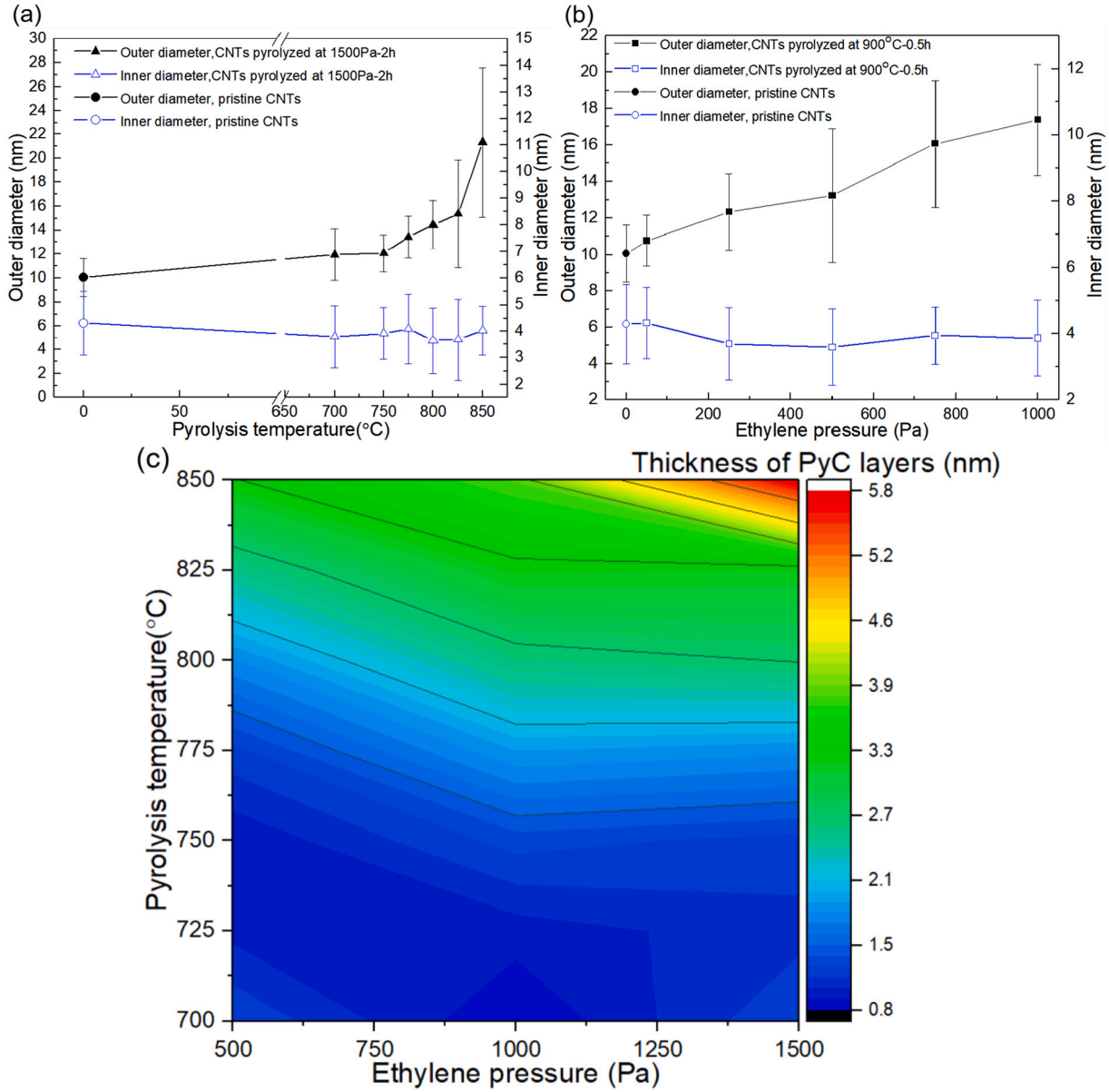

Fig. 2. (a) Relation between the outer/inner diameters of PyC-coated CNTs and the pyrolysis temperature; (b) Relation between the outer/inner diameters of PyC-coated CNTs and the ethylene pressure; (c) The colorful contour map shows the deposition thickness of PyC layers under different temperatures and ethylene pressures (fixing the growth time at 2 h).

comparing the wall thickness ($\frac{D-d}{2}$) of the PyC-coated CNTs with that of the pristine CNT sample, the average deposition thickness of PyC layers can be calculated. The contour map of the PyC thickness is plotted as a function of pyrolysis temperature and ethylene pressure (Fig. 2c). Note that when the pyrolysis temperature is above 825 °C, the deposition thickness of PyC layers remarkably increases with the rising ethylene pressure. However, the increase of PyC layer thickness is not obvious with the increasing ethylene pressure when the temperature is below 750 °C. Such a phenomenon may be explained by the saturated adsorption of hydrocarbon molecules at the CNT surface under relatively low temperatures [7].

Considering the ethylene pressure used in this study (0.05–1.5 kPa), small carbon species C_n ($n = 1, 2 \ldots$) may be the main pyrolysis products at low pressures [25,26], which are different from the polyaromatic hydrocarbons (PAHs) usually produced under the high-pressure pyrolysis of hydrocarbons [27]. Some experimental works [28,29] have indicated that the PyC layers assembled from PAHs may be inclined to exhibit a disordered or even amorphous microstructure. In comparison, Chen et al. [30] suggested that the self-assembly of small carbon species can achieve an intact in-plane architecture such as the well-aligned graphitic layers, which is probably one merit of the low-pressure vapor growth. In our experiments, we observed that the PyC-coated CNTs obtained at 800 °C-1.5 kPa-2 h (Fig. 1d) exhibit a high-stacking morphology of graphitic layers without apparent defects, which is consistent with the simulation study from [30]. Therefore, we choose 800 °C-1.5 kPa as the suitable parameter and set up different growth times to study the growth process and kinetics of epitaxial PyC layers on the CNT template.

Various morphologies of the PyC-coated CNTs after different growth times at 800 °C-1.5 kPa are shown in Fig. 3a–f. The yellow dashes indicate the outline of pristine CNTs while the blue arrows indicate the deposition thickness of PyC layers. As the growth time increases from 1 h to 12 h, the thickness of PyC layers increases from 2 nm to nearly 20 nm. In Fig. 3a–b, the deposited PyC layers show the well-aligned morphology, which is consistent with our previous report [18] of

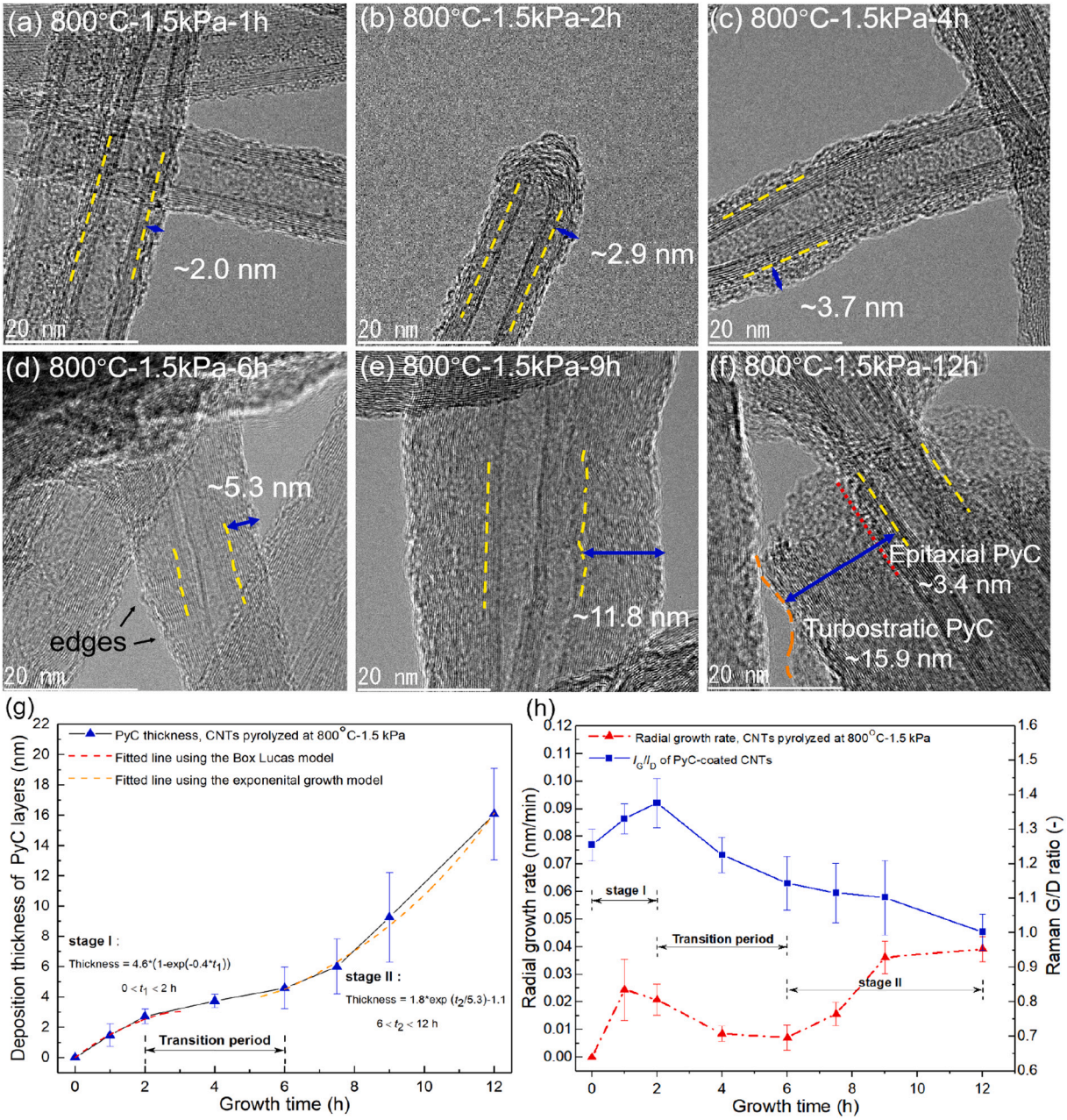

Fig. 3. (a)–(f) TEM images of the PyC-coated CNTs after different growth times (fixing the temperature at 800 °C, the ethylene pressure at 1.5 kPa); (g) Relation between the deposition thickness of PyC layers and the growth time; (h) Influence of the growth time on the radial growth rate and the Raman G/D ratio of PyC-coated CNTs, respectively.

epitaxial graphene shells grown at the surface of defective CNTs. In Fig. 3d, we can observe that the growing edges are exposed at the outermost surface of PyC-coated CNTs. In Fig. 3e, the deposited PyC layers obviously become disordered. Interestingly, we notice the fracture morphology (Fig. 3f) of a thick PyC-coated CNT sample. The fracture may result from the ultrasonic dispersion during the TEM sample preparation. We infer that there exists the mechanical strength difference between the inner un-fractured PyC layers (between the yellow dash and the red dot line) and the outer fractured PyC layers (between the red dot line and the orange dash). In other words, there are probably two microstructures co-existing in the thick PyC coating on CNT surfaces. Zhang et al. [31] reported the dual-phase microstructure at the interface region of CNT/C composites, in which the interface transition starts from CNT walls, to well-aligned epitaxial graphitic layers, finally to the disordered carbons. Whereas, the interface bonding strength between the disordered carbon layers and the well-aligned graphitic layers may be weak [32], which plausibly supports our observation of the fracture morphology in Fig. 3f.

Therefore, we conducted XRD and Raman characterization of the PyC-coated CNT samples to confirm the microstructural difference induced by the growth time. The typical XRD and Raman spectra can be found in Fig. S4 (Supplementary material). Using the Bragg equation [16], we calculated the average interlayer spacing (d_{002}) based on the position of (002) peak from the XRD spectra. Using the Scherrer equation [33], we calculated the average crystallite thickness (L_c), crystallite size (L_a) based on the peak position and the full width at half maximum of (002) or (100) peaks, respectively. The structural parameters are summarized in Table 1. When the growth time of PyC-coated CNTs is less than 2 h, these samples show the similar interlayer spacing (d_{002}) and the increased crystallite dimension (L_a and L_c) compared with the

Table 1
Microstructural parameters of the PyC-coated CNTs (pyrolyzed at 800 °C-1.5 kPa of ethylene) as the growth time increases: interlayer spacing (d_{002}), crystallite thickness (L_c) and crystallite size (L_a) obtained from the XRD spectra; integrated intensity ratio (I_G/I_D), full width at half-maximum of G-peak (G-FWHM) obtained from the Raman spectra.

CNT sample	XRD			Raman	
	d_{002} (nm)	L_c (nm)	L_a (nm)	I_G/I_D	G-FWHM (cm^{-1})
Pristine	0.340	2.9	4.2	1.26	58.92
800 °C-1.5 kPa-1 h	0.340	3.5	12.2	1.33	58.24
800 °C-1.5 kPa-2 h	0.340	4.1	16.1	1.38	55.84
800 °C-1.5 kPa-4 h	0.341	4.2	11.7	1.23	67.80
800 °C-1.5 kPa-6 h	0.341	4.1	10.0	1.14	68.11
800 °C-1.5 kPa-9 h	0.343	3.6	8.2	1.10	70.55
800 °C-1.5 kPa-12 h	0.343	3.6	8.0	1.02	91.06

pristine CNT. However, the crystallite sizes of PyC-coated CNTs show a decreasing trend when the growth time is larger than 4 h, which is consistent with the decreased I_G/I_D and the increase of G-FWHM from Raman spectra, indicating that the crystallinity of PyC layers has decreased. Note that the d_{002} of the PyC-coated CNTs grown at 9 h or 12 h has reached 0.343 nm, exhibiting the propensity of turbostratic carbons. Puech et al. [33] reported that the turbostratic carbons with random stacking order usually exhibit smaller crystallite sizes compared to the graphitic carbons with a highly-oriented stacking order. Thus, we conclude that the un-fractured inner PyC layers in Fig. 3f possess the graphitic microstructure (epitaxial layer thickness ~3.4 nm), and the fractured outer PyC layers may possess a higher density of structural defects (turbostratic layer thickness ~15.9 nm). The mechanism of such a microstructure transition will be discussed later.

The relation between PyC layer thickness and growth time is plotted in Fig. 3g, clearly showing a nonlinear two-stage behavior. We fitted the curves in stage I and stage II based on the Box Lucas model and the exponential growth model, respectively. Here we define that there is a transition period between stage I and stage II, during which the growth rate firstly decreases and then starts to increase. In Fig. 3h, the red dashes plot the relation between the radial growth rate of PyC layers and growth time, while the solid blue lines plot the relation between the I_G/I_D of PyC-coated CNTs and growth time. I_G/I_D and the growth rate both exhibit a non-monotonic behavior, implying that the growth rate may correlate with the Raman G/D ratio. It is well-known that the density of defective sites on graphite surfaces is inversely proportional to I_G/I_D [34]. Some studies [35,36] have discussed the CNT defective locations as the inherent active sites to adsorb molecules and to catalyze chemical reactions. Thus, we may assume that the defect density of CNT surfaces can affect the decomposition speed of hydrocarbon molecules and consequently influence the dominating reaction pathways.

Based on the above results, next we discuss the possible reaction pathways during the low-pressure vapor deposition of PyC layers on CNTs (Fig. 4a). We proposed our growth model (Fig. 4b) to explain the two-stage growth kinetics of PyC layers on the CNT template. Note that our radial growth model focuses on the carbon layer deposition on CNT external surfaces induced by gas-phase pyrolysis; the mechanism of CNT tip growth and of the layer growth inside CNT channels during the hydrocarbon pyrolysis can be found elsewhere [37,38].

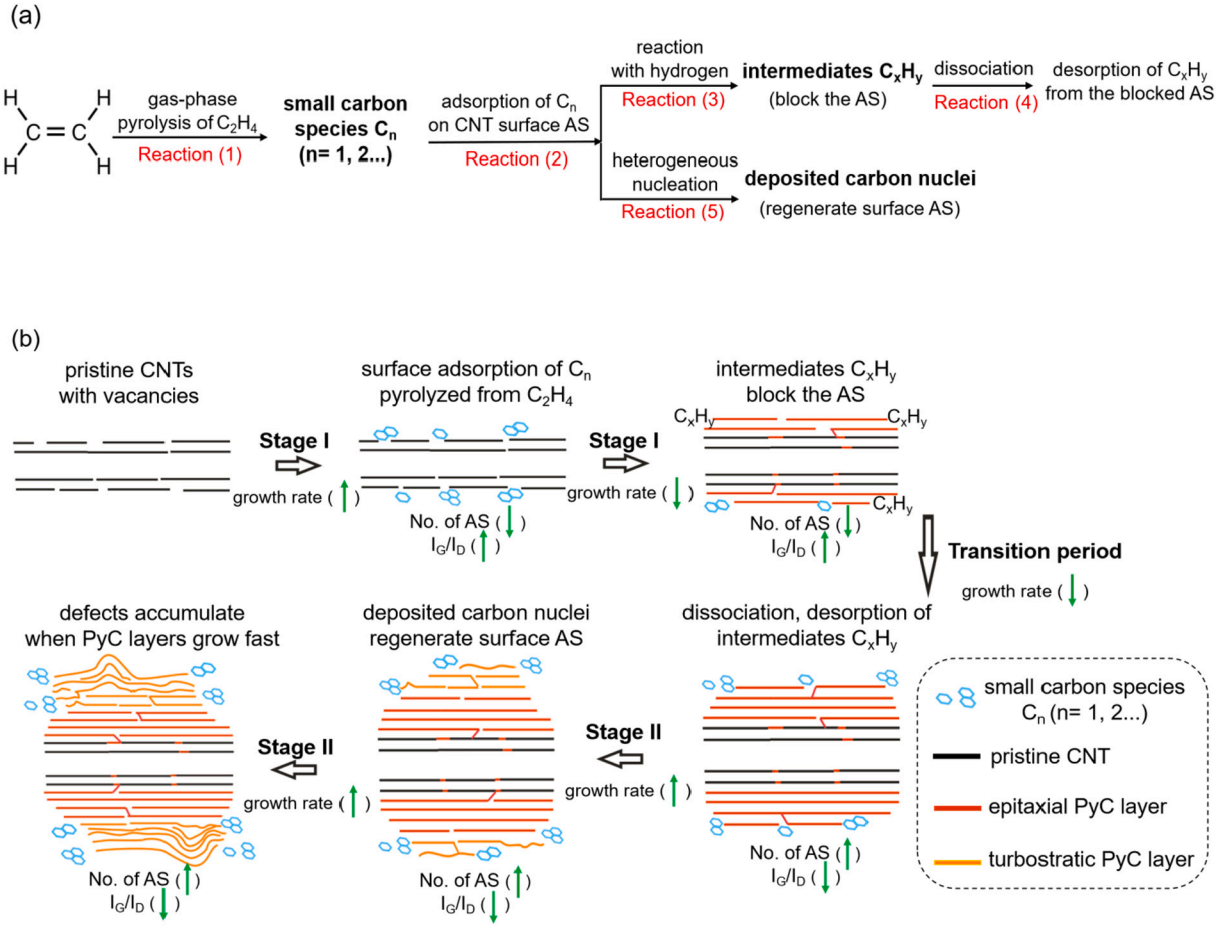

Fig. 4. (a) The suggested reaction pathways to explain the growth kinetics of PyC layers on CNT outer surfaces; (b) Illustration of the radial growth process of PyC layers deposited on the CNT template. In this figure, the active site and the number of active sites are abbreviated as "AS" and "No. of AS", respectively.

3.1. Stage I

As shown in Fig. 4a, small carbon species (C_n) may be produced from the gas-phase pyrolysis of ethylene (Reaction (1)). The chemisorption of small carbon species onto the CNT active sites (Reaction (2)) results from the impingement between carbon radicals and dangling bonds of vacancies, which is beneficial to the surface nucleation at the initial stage [39]. It corresponds to the initial growth of PyC layers in a layer-by-layer mode. When nearly all the vacancy sites are occupied, the layer crystallinity can slightly increase due to the edge saturation of the graphene lattice. Our experimental results show that the growth rate of PyC layers gradually decreases in stage I, so the adsorption of small carbon species is inferred to slow down, affected by the lack of available active sites on CNT surfaces [40]. Also, interaction between reaction byproducts may generate hydrocarbon complex intermediates (C_xH_y), which was reported to effectively block the active sites and inhibit the carbon deposition [41]. Note that the buildup of hydrocarbon intermediates (Reaction (3)) and the deposition of carbon nuclei (Reaction (5)) usually do not take place at the same active site. We suggest that it is possible to additionally prolong the duration of stage I by surface cleaning techniques (e.g., plasmon-assisted activation) at the end of stage I, because it may remove the surface-adhered hydrocarbon intermediates and regenerate the active sites. Promisingly, the prolonged stage I can further increase the thickness of epitaxial graphitic layers with the crystallinity that is comparable to the crystallinity of pristine CNT walls.

3.2. Transition period

Two typical features of the transition period are the decrease of coating crystallinity (I_G/I_D) and the reduction of radial growth rate. As shown in Fig. 3h, the growth rate does not immediately increase along with the increase of defect densities (decreased I_G/I_D), implying the complicated reactions during the transition period. When the transition period ends, the radial growth rate starts to recover. Presumably the occurrence of transition period is related with the regeneration behavior of the active sites on PyC-coated CNT surfaces. We noticed the existence of opening edges (Fig. 3d) at the outermost surface of PyC-coated CNTs during the transition period. More importantly, the accumulation of opening edges with the increasing number of unsaturated atoms may generate some chemical reaction sites [42] that promote the dissociation of surface-adhered hydrocarbon intermediates (reaction (4)). According to our experimental studies of the PyC-coated CNTs at different growth times (800 °C-1.5 kPa), the transition period is as long as 4 h. As reported by [41], the effective dissociation and desorption of hydrocarbon intermediates to regenerate active sites might be a slow process because of the firm bonding between the intermediates and the substrate layer. Therefore, we assume that the transition period might terminate only if the concentration of available active sites on the carbon substrate layer is accumulated to a threshold level [43].

3.3. Stage II

As illustrated in Fig. 4b, the important features of stage II are the increase of growth rate and the decrease of coating crystallinity (I_G/I_D). We infer that the self-assembly growth of PyC layers during the low-pressure vapor deposition is dependent on the number of surface active sites (defective sites). Indeed, the crystallinity of the PyC-coated CNTs in stage II significantly decreases as the PyC thickness rapidly increases, indicating the defect-related growth process. The previous study [43] showed that the nascent CNTs can quickly grow because incomplete side walls and open edges with the dangling bonds can efficiently incorporate the carbon clusters into the hexagonal network. In addition, the surface area of the outermost CNT wall has been reported [9] to increase significantly with regard to the increasing CNT outer diameter. Thus, the enlarging surface area of the outermost carbon layer combined with the increasing defect density can significantly increase the number of available active sites, which enhances the speed of adsorption (Reaction (2)) and nucleation (Reaction (5)) of carbon species at the surface active site [44]. However, due to the accumulation of structural defects during the fast growth process, the microstructure of the deposited PyC layers in stage II becomes more disordered compared to that in stage I, which can explain the microstructure transition from the inner graphitic layers to the outer turbostratic layers as revealed by Fig. 3f and Table 1. We suggest that the high-temperature annealing of the PyC-coated CNTs after stage II can effectively increase the sample crystallinity because the defect-healing effect by high-temperature annealing has been verified by some previous studies [15,16,45].

Our experimental results seem to contradict with the statement [32] saying that non-catalytic growth of graphene layers on CNT surfaces cannot occur below 1100 °C. Here we suggest that the self-assembly of crystalline graphitic carbon on CNT surfaces is possible even under the low-temperature and low-pressure pyrolysis of ethylene. Based on our findings, the thickness of epitaxial PyC layers deposited on CNTs can be adjusted by simply changing the growth time under typical pyrolysis conditions, which may offer a cost-effective way to tailor the wall number of CVD-grown CNTs. Our recent work of the molecular dynamics simulation [46] has proved that precisely controlling the wall number of thin-walled CNTs can tailor the effective loading area under tensile forces and consequently improve the nominal (engineering) tensile strength of CNTs, which may be essential for the high-strength CNT-based composites. Moreover, we propose that the epitaxial deposition of the graphitizable carbon layers onto the defective CNT surfaces can promote the defect-healing effect and tensile property improvement of the high-temperature annealed CVD-grown CNTs [11].

4. Conclusions

In this study, the non-catalytic pyrolysis of ethylene at low pressures has realized the epitaxial growth of pyrolytic carbon (PyC) layers at the CNT surface. The self-assembly growth of PyC layers essentially results from the dissociative adsorption, coalescence, and nucleation of small carbon species at the surface active sites, so the number of active sites significantly influences the growth rate of PyC layers. We propose a radial growth model to explain the two-stage growth kinetics of the PyC-coated CNTs. The epitaxial deposition of PyC layers on the CNT template is expected to offer one simple and useful way for adjusting the wall number (diameter) of multi-walled CNTs. Moreover, this study may provide some insights into the self-assembly mechanism of CNTs (or graphenes) grown on the non-metallic substrate.

CRediT authorship contribution statement

Conceptualization, Fan Liu; Methodology, Fan Liu and Naoto Nishioka; Writing-original draft preparation, Fan Liu; Writing-review & editing, Fumio Ogawa and Toshiyuki Hashida; Funding acquisition, Fumio Ogawa and Toshiyuki Hashida. All authors have read and agreed to the submitted version of the manuscript.

Declaration of competing interest

The authors declare that they have no known competing financial interests or personal relationships that could have appeared to influence the work reported in this paper.

Acknowledgments

The authors thank Dr. T Miyazaki from the Technical Division, School of Engineering, Tohoku University for technical assistance in TEM analysis; we thank Lintec of America, Inc., Nano-Science & Technology Center (NSTC) for supplying the MWCNT sheets. This work was supported by JSPS KAKENHI Grant Numbers JP19K14837 and

JP21K14489.

Appendix A. Supplementary data

Supplementary data to this article can be found online at https://doi.org/10.1016/j.diamond.2022.108857.

References

[1] V. Jourdain, C. Bichara, Current understanding of the growth of carbon nanotubes in catalytic chemical vapour deposition, Carbon 58 (2013) 2–39, https://doi.org/10.1016/j.carbon.2013.02.046.

[2] G.D. Nessim, A.J. Hart, J.S. Kim, D. Acquaviva, J. Oh, C.D. Morgan, M. Seita, J. S. Leib, C.V. Thompson, Tuning of vertically-aligned carbon nanotube diameter and areal density through catalyst pre-treatment, Nano Lett. 8 (2008) 3587–3593, https://doi.org/10.1021/nl801437c.

[3] M. Kumar, Y. Ando, Chemical vapor deposition of carbon nanotubes: a review on growth mechanism and mass production, J. Nanosci. Nanotechnol. 10 (2010) 3739–3758, https://doi.org/10.1166/jnn.2010.2939.

[4] O. Yaglioglu, A. Cao, A.J. Hart, R. Martens, A.H. Slocum, Wide range control of microstructure and mechanical properties of carbon nanotube forests: a comparison between fixed and floating catalyst CVD techniques, Adv. Funct. Mater. 22 (2012) 5028–5037, https://doi.org/10.1002/adfm.201200852.

[5] G.S. Duesberg, A.P. Graham, M. Liebau, R. Seidel, E. Unger, F. Kreupl, W. Hoenlein, Growth of isolated carbon nanotubes with lithographically defined diameter and location, Nano Lett. 3 (2003) 257–259, https://doi.org/10.1021/nl025906c.

[6] W.H. Chiang, D.N. Futaba, M. Yumura, K. Hata, Growth control of single-walled, double-walled, and triple-walled carbon nanotube forests by a priori electrical resistance measurement of catalyst films, Carbon 49 (2011) 4368–4375, https://doi.org/10.1016/j.carbon.2011.06.015.

[7] X. Feng, K. Liu, X. Xie, R. Zhou, L. Zhang, Q. Li, S. Fan, K. Jiang, Thermal analysis study of the growth kinetics of carbon nanotubes and epitaxial graphene layers on them, J. Phys. Chem. C 113 (2009) 9623–9631, https://doi.org/10.1021/jp901245u.

[8] G. Bin Zheng, H. Sano, Y. Uchiyama, A layer-by-layer deposition mechanism for producing a pyrolytic carbon coating on carbon nanotubes, Carbon 57 (2013) 267–273, https://doi.org/10.1016/j.carbon.2013.01.073.

[9] D.V. Krasnikov, V.L. Kuznetsov, A.I. Romanenko, A.N. Shmakov, Side reaction in catalytic CVD growth of carbon nanotubes: surface pyrolysis of a hydrocarbon precursor with the formation of lateral carbon deposits, Carbon 139 (2018) 105–117, https://doi.org/10.1016/j.carbon.2018.06.033.

[10] M. Monthioux, H. Allouche, R.L. Jacobsen, Chemical vapour deposition of pyrolytic carbon on carbon nanotubes. Part 3: growth mechanisms, Carbon 44 (2006) 3183–3194, https://doi.org/10.1016/j.carbon.2006.07.001.

[11] F. Liu, K. Shirasu, T. Hashida, Epitaxial pyrolytic carbon coatings templated with defective carbon nanotube cores for structural annealing and tensile property improvement, J. Mater. Sci. 56 (2021) 19015–19028, https://doi.org/10.1007/S10853-021-06523-8.

[12] S.R.C. Vivekchand, A. Govindaraj, M.M. Seikh, C.N.R. Rao, New method of purification of carbon nanotubes based on hydrogen treatment, J. Phys. Chem. B 108 (2004) 6935–6937, https://doi.org/10.1021/jp048737o.

[13] O. Yildiz, P.D. Bradford, Aligned carbon nanotube sheet high efficiency particulate air filters, Carbon 64 (2013) 295–304, https://doi.org/10.1016/j.carbon.2013.07.066.

[14] R. Xiang, Z. Yang, Q. Zhang, G. Luo, W. Qian, F. Wei, M. Kadowaki, E. Einarsson, S. Maruyama, Growth deceleration of vertically aligned carbon nanotube arrays: catalyst deactivation or feedstock diffusion controlled? J. Phys. Chem. C 112 (2008) 4892–4896, https://doi.org/10.1021/jp710730x.

[15] S. Faraji, K. Stano, C. Rost, J.P. Maria, Y. Zhu, P.D. Bradford, Structural annealing of carbon coated aligned multi-walled carbon nanotube sheets, Carbon 79 (2014) 113–122, https://doi.org/10.1016/j.carbon.2014.07.049.

[16] S. Faraji, O. Yildiz, C. Rost, K. Stano, N. Farahbakhsh, Y. Zhu, P.D. Bradford, Radial growth of multi-walled carbon nanotubes in aligned sheets through cyclic carbon deposition and graphitization, Carbon 111 (2017) 411–418, https://doi.org/10.1016/j.carbon.2016.10.012.

[17] R. Zhong, R. Hong, Continuous preparation and formation mechanism of few-layer graphene by gliding arc plasma, Chem. Eng. J. 387 (2020), 124102, https://doi.org/10.1016/j.cej.2020.124102.

[18] K. Shirasu, M. Asaoka, T. Miyazaki, G. Yamamoto, T. Hashida, Stack-coating of multishell carbon layers templated with carbon nanotubes, Mater. Today Commun. 21 (2019), 100608, https://doi.org/10.1016/j.mtcomm.2019.100608.

[19] P.R. Mudimela, A.G. Nasibulin, H. Jiang, T. Susi, D. Chassaing, E.I. Kauppinen, Incremental variation in the number of carbon nanotube walls with growth temperature, J. Phys. Chem. C 113 (2009) 2212–2218, https://doi.org/10.1021/jp808316p.

[20] M.P. Siegal, D.L. Overmyer, P.P. Provencio, D.R. Tallant, Linear behavior of carbon nanotube diameters with growth temperature, J. Phys. Chem. C 114 (2010) 14864–14867, https://doi.org/10.1021/jp105815u.

[21] Y. Van De Burgt, Y. Bellouard, R. Mandamparambil, Kinetics of laser-assisted carbon nanotube growth, Phys. Chem. Chem. Phys. 16 (2014) 5162–5173, https://doi.org/10.1039/c4cp00061g.

[22] G. Abadias, E. Chason, J. Keckes, M. Sebastiani, G.B. Thompson, E. Barthel, G. L. Doll, C.E. Murray, C.H. Stoessel, L. Martinu, Review article: stress in thin films and coatings: current status, challenges, and prospects, J. Vac. Sci. Technol., A 36 (2018), 020801, https://doi.org/10.1116/1.5011790.

[23] F.C. Marques, R.G. Lacerda, A. Champi, V. Stolojan, D.C. Cox, S.R.P. Silva, Thermal expansion coefficient of hydrogenated amorphous carbon, Appl. Phys. Lett. 83 (2003) 3099, https://doi.org/10.1063/1.1619557.

[24] H. Allouche, M. Monthioux, Chemical vapor deposition of pyrolytic carbon on carbon nanotubes. Part 2. Texture and structure, Carbon 43 (2005) 1265–1278, https://doi.org/10.1016/j.carbon.2004.12.023.

[25] T. Kunugi, T. Sakai, K. Soma, Y. Sasaki, Kinetics and mechanism of the thermal reaction of ethylene, Ind. Eng. Chem. Fundam. 8 (1969) 374–383, https://doi.org/10.1021/i160031a002.

[26] Y. Yamamoto, S. Inoue, Y. Matsumura, Thermal decomposition products of various carbon sources in chemical vapor deposition synthesis of carbon nanotube, Diam. Relat. Mater. 75 (2017) 1–5, https://doi.org/10.1016/j.diamond.2016.11.017.

[27] G. Paredes, T. Ondarçuhu, M. Monthioux, F. Piazza, Unveiling the existence and role of a liquid phase in a high temperature (1400 °C) pyrolytic carbon deposition process, Carbon Trends 5 (2021), 100117, https://doi.org/10.1016/j.cartre.2021.100117.

[28] L. Feng, Q. Fu, Q. Song, Y. Yang, Y. Zuo, G. Suo, X. Hou, L. Zhang, X. Ye, A novel continuous carbon nanotube fiber/carbon composite by electrified preform heating chemical vapor infiltration, Carbon 157 (2020) 640–648, https://doi.org/10.1016/j.carbon.2019.11.009.

[29] M. Wang, J. Yang, X. You, C. Liao, J. Yan, J. Ruan, S. Dong, Nanoinfiltration behavior of carbon nanotube based nanocomposites with enhanced mechanical and electrical properties, J. Mater. Sci. Technol. 71 (2021) 23–30, https://doi.org/10.1016/j.jmst.2020.07.015.

[30] M.W. Chen, Y.B. Zhu, J. Xia, H.A. Wu, Molecular insights into the initial formation of pyrolytic carbon upon carbon fiber surface, Carbon 148 (2019) 307–316, https://doi.org/10.1016/j.carbon.2019.04.003.

[31] S. Zhang, Y. Ma, L. Suresh, A. Hao, M. Bick, S.C. Tan, J. Chen, Carbon nanotube reinforced strong carbon matrix composites, ACS Nano 14 (2020) 9282–9319, https://doi.org/10.1021/acsnano.0c03268.

[32] K. Li, G. Eres, J. Howe, Y.J. Chuang, X. Li, Z. Gu, L. Zhang, S. Xie, Z. Pan, Self-assembly of graphene on carbon nanotube surfaces, Sci. Rep. 3 (2013) 1–4, https://doi.org/10.1038/srep02353.

[33] P. Puech, A. Dabrowska, N. Ratel-Ramond, G.L. Vignoles, M. Monthioux, New insight on carbonisation and graphitisation mechanisms as obtained from a bottom-up analytical approach of X-ray diffraction patterns, Carbon 147 (2019) 602–611, https://doi.org/10.1016/j.carbon.2019.03.013.

[34] A.C. Ferrari, D.M. Basko, Raman spectroscopy as a versatile tool for studying the properties of graphene, Nat. Nanotechnol. 8 (2013) 235–246, https://doi.org/10.1038/nnano.2013.46.

[35] J. Ortiz-Medina, Z. Wang, R. Cruz-Silva, A. Morelos-Gomez, F. Wang, X. Yao, M. Terrones, M. Endo, Defect engineering and surface functionalization of nanocarbons for metal-free catalysis, Adv. Mater. 31 (2019) 1805717, https://doi.org/10.1002/adma.201805717.

[36] B. Xiao, X. Yu, Y. Ding, Theoretical investigation on the healing mechanism of divacancy defect in CNT growth by C2H2 and C2H4, J. Mol. Model. 20 (2014) 1–8, https://doi.org/10.1007/S00894-014-2125-8.

[37] M. Endo, K. Takeuchi, K. Kobori, K. Takahashi, H.W. Kroto, A. Sarkar, Pyrolytic carbon nanotubes from vapor-grown carbon fibers, Carbon 33 (1995) 873–881, https://doi.org/10.1016/0008-6223(95)00016-7.

[38] N. Gilani, J.T. Daryan, A. Rashidi, M.R. Omidkhah, Separation of methane-nitrogen mixtures using synthesis vertically aligned carbon nanotube membranes, Appl. Surf. Sci. 258 (2012) 4819–4825, https://doi.org/10.1016/j.apsusc.2012.01.126.

[39] F. Scholz, Active sites of heterogeneous nucleation understood as chemical reaction sites, Electrochem. Commun. 13 (2011) 932–933, https://doi.org/10.1016/j.elecom.2011.06.003.

[40] W.P. Hoffman, F.J. Vastola, P.L. Walker, Pyrolysis of propylene over carbon active sites-I.Kinetics, Carbon 23 (1985) 151–161, https://doi.org/10.1016/0008-6223(85)90006-5.

[41] R. Venkateswaran, M.H. Back, G. Scacchi, The dual nature of carbon: catalyst and inhibitor, Carbon 32 (1994) 911–919, https://doi.org/10.1016/0008-6223(94)90048-5.

[42] W.P. Hoffman, F.J. Vastola, P.L. Walker, Pyrolysis of propylene over carbon active sites II.Pyrolysis products, Carbon 26 (1988) 485–499, https://doi.org/10.1016/0008-6223(88)90147-9.

[43] G. Eres, C.M. Rouleau, M. Yoon, A.A. Puretzky, J.J. Jackson, D.B. Geohegan, Model for self-assembly of carbon nanotubes from acetylene based on real-time studies of vertically aligned growth kinetics, J. Phys. Chem. C 113 (2009) 15484–15491, https://doi.org/10.1021/jp9001127.

[44] E. Bouchard, J. Lavenac, J.-C. Roux, F. Langlais, P. Delha⟩s, Pyrocarbon deposits on a graphite surface observed by STM, **, Chem. Vap. Depos. 7 (2001) 125–130, https://doi.org/10.1002/1521-3862(200105)7:3<125::AID-CVDE125>3.0.CO;2-B.

[45] X. Lin, W. Zhao, W. Zhou, P. Liu, S. Luo, H. Wei, G. Yang, J. Yang, J. Cui, R. Yu, L. Zhang, J. Wang, Q. Li, W. Zhou, W. Zhao, S. Fan, K. Jiang, Epitaxial growth of aligned and continuous carbon nanofibers from carbon nanotubes, ACS Nano 11 (2017) 1257–1263, https://doi.org/10.1021/acsnano.6b04855.

[46] K. Shirasu, S. Kitayama, F. Liu, G. Yamamoto, T. Hashida, Molecular dynamics simulations and theoretical model for engineering tensile properties of single-and multi-walled carbon nanotubes, Nanomaterials. 11 (2021) 795, https://doi.org/10.3390/nano11030795.